Couplings between a resonant current source power supply and a DBD excilamp

Hubert Piquet, D Florez, X. Bonnin, Antoine Belinger, R Diez

Couplings between a resonant current source power supply and a DBD excilamp

H. Piquet[1], D. Florez[2], X. Bonnin[1], A. Belinger[3], R. Diez[2]*

[1] Institution Toulouse University. Institut National Polytechnique de Toulouse
2 rue Camichel-31071 Toulouse cedex, France
[2] Pontificia Universidad Javeriana
Carrera 7, N 40–62 Faculdad de Ingenieria-110231 Bogotá, Colombia
[3] Toulouse University. Université Paul Sabatier
118, route de Narbonne-31062 Toulouse cedex 9, France

Поступила в редакцию 6.03.2014 г.

This paper presents a study of couplings which take place in systems where dielectric barrier discharge (DBD) excimer lamps are supplied with current source electrical power generators. Causal analysis, using the fundamental properties of the DBD, is used for the design of such current sources. A two steps approach is developed here: in order to control the lamp power, with the best efficiency concerning the UV emission, a current shape controlled current generator is set-up to investigate the possible degrees of freedom of the current waveforms: frequency, peak current, pulse duration.

On this basis, "optimized" supplying conditions are selected, and a second power generator with high electrical efficiency is designed: its operating mode combines discontinuous current mode and soft-commutation (ZCS), obtaining as well low electromagnetic emissions and reduced switching losses. A classical electrical equivalent model of the lamp is used to achieve the state plane analysis and to calculate all the electric variables involved in the design of the converter and consequently to select its components. The mathematical relationships obtained from this process, especially those concerning the control of the injected power by means of the available degrees of freedom, are validated with simulations and experimental results. Experimental UV emission performances are presented as well.

Keywords: dielectric barrier discharge, excimer lamps, power supply, optimization, resonant inverter, UV.

Introduction

Excimer lamps are powerful and flexible emitters of narrow band UV radiations [1, 2], which applications are currently more and more spreading out [3]. In the current context of transition from fundamental studies to industrial applications, the efficiency and controllability of the UV emission is of more and more important concern. In this aim, the study which is presented in this paper is focused on the definition of the most fitted characteristics of the electrical power generator associated to the lamp.

The choice of the characteristics of the power supplies for dielectric barrier discharge devices, and especially for DBD excilamps, has been shown in a number of previous papers to be of crucial importance for the overall system's performances.

For instance, on the basis of the classical equivalent circuit of DBD devices [4, 5], which is reminded in Fig. 1, the comparison of the electrical simulation waveforms, obtained with pulsed voltage of pulsed current generators (square shapes) is exhibited in Fig. 2.

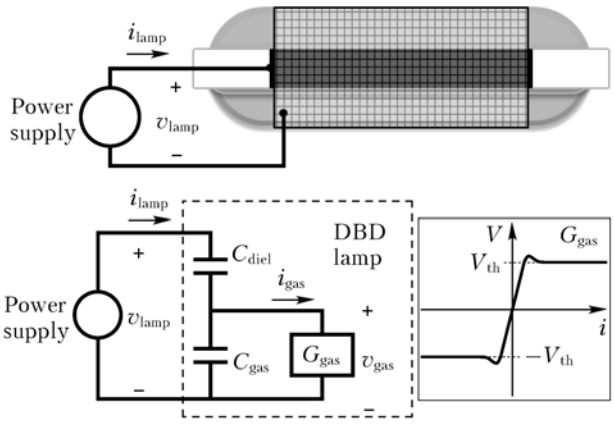

Fig. 1. DBD excilamp. Structure and electrical model

For these numerical simulations, the parameters of the equivalent circuit are adjusted to reflect the operation of a 100 W bulb filled with a $Xe–Cl_2$ mixture (wavelength is 308 nm). The following values from Table 1 are taken into account; concerning the conductance of the gas in *ON* state, the voltage plateau across the latter is assumed to remain at the same V_{th} level as at the threshold time.

Although pulsed voltage sources have shown to be a performing solution at the experimental investigation's step, a more reliable design and a tighter control of the performances are needed for industrial

* Hubert Piquet (Hubert.Piquet@laplace.univ-tlse.fr); David Florez (d.florez@javeriana.edu.co); Xavier Bonnin (Xavier.Bonnin@laplace.univ-tlse.fr); Antoine Belinger (Antoine.Belinger@laplace.univ-tlse.fr); Rafael Diez (rdiez@javeriana.edu.co).

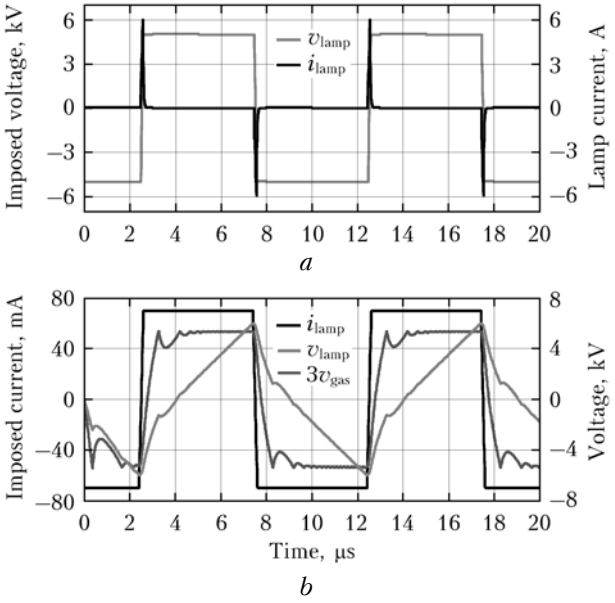

Fig. 2. Voltage-mode converter with square voltage output and uncontrolled current (*a*), and current-mode converter with square current and controlled voltage (*b*) — theoretical simulation waveforms

Table 1

Equivalent electrical parameters of a Xe–Cl_2 DBD excilamp

Symbol	Parameter	Value
V_{th}	Threshold voltage — plateau level	1310 V
C_{diel}	Dielectric barriers capacitance	85 pF
C_{gas}	Gas gap capacitance	28 pF
P_{lamp}	Nominal lamp power	100 W

applications [2, 6, 7]. Indeed, the actual control of the power injected into the lamp by such a pulsed voltage generator is really difficult to predict: accounting the capacitive behavior of the DBD system, the magnitude and the duration of the obtained current spikes is related to the slope and the duration of the voltage fronts [8, 9]. The latters are defined by the switching performances of the semiconductors used to produce the pulsed voltage and are really difficult to control in the supplying circuit, from the very first design step.

On the contrary, as illustrated in Fig. 2, *b*, when the current injected into the DBD device is controlled [8, 10], the integral form of the capacitive behavior of the dielectric barriers can be used to define and to predict, from the first design step, the shape and the magnitude of the voltage across both the lamp and the power generator, as well as all the other dimensioning electrical quantities.

1. Current source supply for DBD lamps

In this section, we consider different issues, which are to be accounted when a current source generator is selected to supply a DBD device.

1.1. DBD lamp current shape properties

Taking into account the capacitive behavior of the DBD, whose equivalent circuit (Fig. 1) includes a C_{diel} series capacitor, it is obvious that the average value of the current injected into the lamp, i_{lamp}, needs to be null. If this condition is not fulfilled, the integral term of equation (1), which defines the voltage across the lamp, will take uncontrolled diverging values

$$v_{lamp} = v_{gas} + \frac{1}{C_{diel}} \int i_{lamp}\, dt. \qquad (1)$$

In this scope, a full bridge topology (Fig. 3) is a good candidate to interconnect a current source *J* and the DBD device.

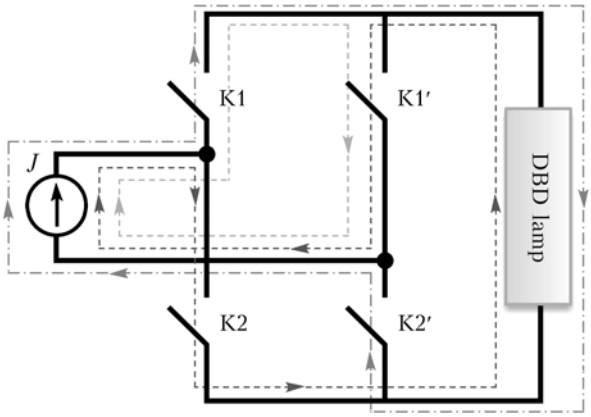

Fig. 3. Bridge configuration, associated with a generic current source to supply a DBD excimer lamp (theoretical step)

Whatever the shape of the *J* current waveform, it offers, according to the different paths which are shown in Fig. 3, three possible values for the i_{lamp} current:

1) $+J$ (when power switches K1 and K2′ are in *ON* state),

2) 0 (if one of the pairs {K1, K1′} or {K2, K2′} is *ON*),

3) $-J$ (when K1′ and K2 are *ON*).

On this basis, the fulfillment of the previous requirement is relatively simple and is mainly a matter of managing the durations of these three sequences.

1.2. Power switches properties

Assuming that the *J* current source is constant and that only $+J$ and $-J$ levels of the i_{lamp} current are used, the following simulatet waveforms (Fig. 4) are presenting the operation of power switches K1 and K2. Similar results are obtained for power switches K4 and K3.

These waveforms are highlighting the need of thyristor-like devices [11], according to the following elements of the simulated behavior, as summarized in Fig. 5:

1) bidirectional voltage (*OFF* state),

2) controlled turn-on under positive voltage,

3) positive current conductive sequence (*ON* state),

4) spontaneous turn-off, leading to negative voltage.

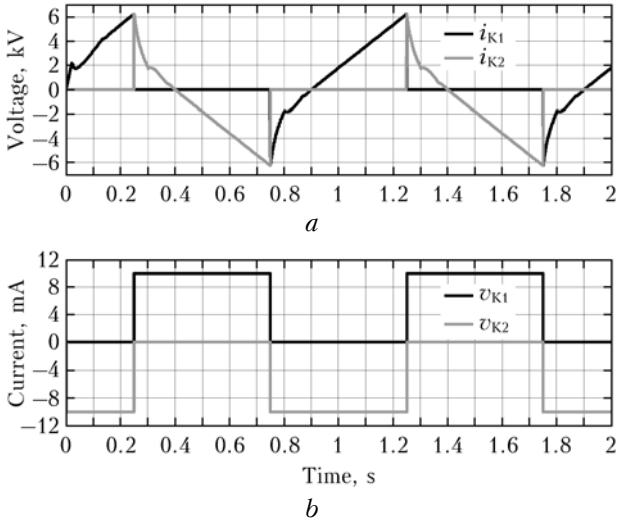

Fig. 4. Simulated waveforms of voltage (*a*) and current (*b*) of both K1 (black) and K2 (grey) power switches

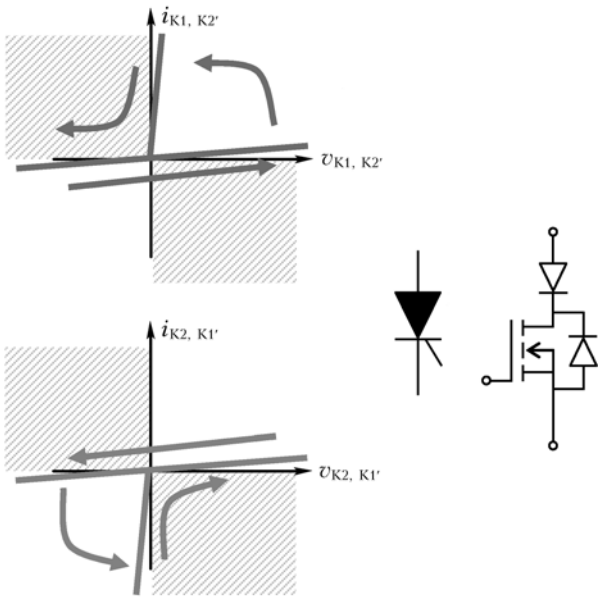

Fig. 5. Operating characteristics of K1 and K2 power switches

Taking also into account that the operating frequencies will be in the 10–200 kHz range, actual thyristor devices are not fitted and synthesized solutions need to be set up, with a mosfet-diode series association.

1.3. High voltage step-up transformer

Considering the voltage levels which are presented on the waveforms of Fig. 4, usual MOSFETs and diodes are not adapted. For this reason, a step-up $1:n$ transformer needs to be introduced in the system. This device is inserted between the DBD lamp and the full bridge converter (Fig. 6); it reduces in an n ratio the voltages which are seen across the terminals of the bridge devices.

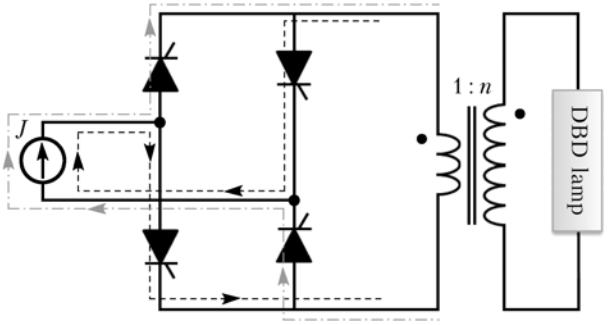

Fig. 6. Thyristor-like devices full bridge configuration, connected to the DBD excimer lamp, through a step-up high voltage transformer

According to the voltage levels which are expected across the lamp (i.e., 4–5 kV), a ratio value 1 : 10 to 1 : 12 is selected.

Effect of the parasitic capacitance of the HV transformer

Since the DBD lamp is an electrical load of capacitive nature and its capacitances are in the order of pF (see Table 1), the design of the transformer is a key aspect for the good performance of the power supply. As a matter of fact, the inter-winding capacitances of the transformer strongly decrease the power injected in the DBD [10]. Assuming that the transformer is highly coupled, that the study focuses only on low frequency phenomena (e.g., which do not involve the leakage inductance), and that the inter-winding voltage V_{ps} is well defined, the high voltage transformer can be modeled by the scheme presented in Fig. 7, where V_{ps} is assumed to be proportional to the secondary potential V_2 in order to take into account several connection schemes.

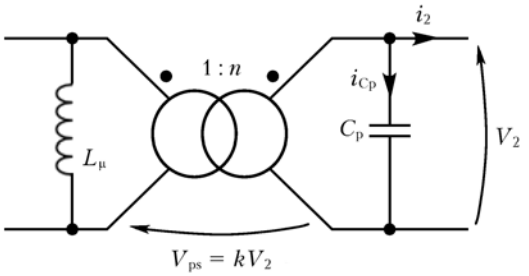

Fig. 7. Low frequency equivalent circuit (primary voltage is neglected, when compared to the secondary one) of the high voltage transformer

If C_p is comparable to the lamp equivalent capacitance, a current divider effect takes place and a considerable amount of the supply output current is derived through C_p, penalizing the efficiency or even forbidding the lamp ignition.

Fig. 8 presents the current of the lamp for two different value of the C_p capacitance (simulation results). One can notice the distortion of the expected square shape current injected into the DBD lamp. The latter takes place at the moment of the change of the direction of the current (by mean of the inverter presented in P. 1.1).

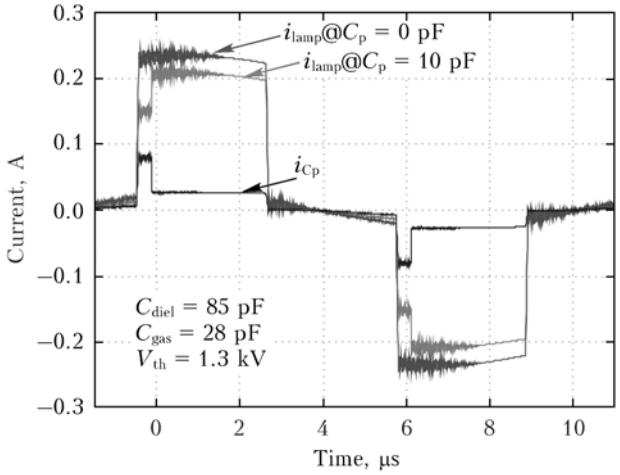

Fig. 8. Distortion of the square current injected into the DBD lamp, due to the C_p parasitic capacitance of the high voltage transformer

This phenomenon provokes a delay of the associated ignition of the plasma (indeed, the gas voltage needs to change from $+V_{th}$ to $-V_{th}$, or, vice versa, as a result of the charge transfer which takes place in the C_{gas} capacitance).

Elements for the design of the HV transformer

On the basis of analytical calculations, the electrostatic energy W which is stored in the volume of the transformer is calculated [12]. This calculation takes into account the geometrical and physical parameters of the transformer, but also the way the secondary potential is related to the primary one through V_{ps}. According to Fig. 7, the electrostatic energy stored into the transformer W, can be expressed by:

$$W = \frac{1}{2} C_p V_2^2, \qquad (2)$$

where C_p explicitly depends on k and on the transformer building parameters (the way the turns are arranged, the number of layers, the insulation layers materials and thicknesses, etc.). Given the small value of the lamp equivalent capacitance (see Table 1), a low transformer's output capacitance C_p is mandatory; in order to minimize C_p, several winding configurations have to be considered. The secondary winding can be split in several sections (Fig. 9).

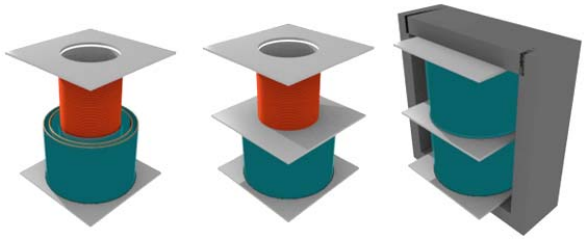

Fig. 9. Organization of the windings of the high-voltage step up transformer: high voltage winding is organized in sections (here, 2 sections). Each section gathers turn layers separated by insulating tapes

On the basis of analytical calculations, using the geometrical properties of the arrangements of the windings (Fig. 9), the electrostatic energy W which is stored in the volume of the transformer (i.e., volume of the windings layers, insulations layers, free space between the windings and the core) is calculated [12]. This calculation takes into account the V_{ps} potential of the secondary winding with respect to the primary one, thus accounting for grounding properties.

Being an analytical expression which incorporates the winding organization and the transformer's geometrical parameters, C_p is used to implement an optimizing algorithm which helps in designing the windings to minimize the parasitic effects.

The step-up ratio being chosen, for a fixed magnetic core, a fixed number of turns, a fixed number of layers, and a fixed amount of insulation material, the theoretical study of [12] shows that splitting the secondary winding allows reducing the value of C_p and that there is an optimal way to define the secondary winding potential through the value of k.

In Fig. 10, the "W versus k" curves of a particular four-layers high voltage step-up transformer are compared for several numbers of sections (which are connected in series).

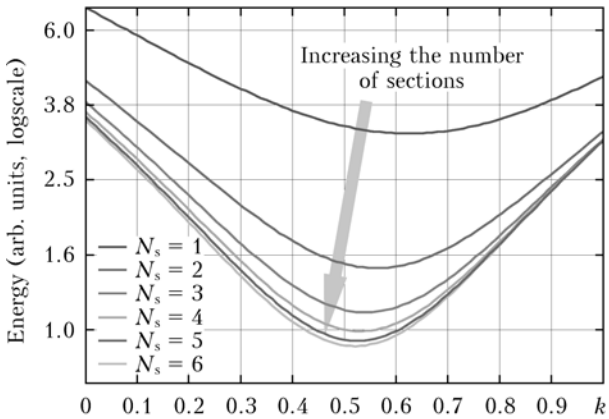

Fig. 10. Optimization of the winding's arrangement (N_1 = 4)

The value of C_p can be reduced by a factor 3 by splitting the secondary winding in four sections and a lower C_p value can be reached by wisely choosing the value of k.

2. Square shape current source supply

In this section, we outline the main properties of a square shape current converter for the supply of DBD lamps; then, we consider the use of the 3 degrees of freedom (DOF) offered by this generator to define the best operating conditions, focusing on the UV emission performances.

2.1. DC current source design

The proposed topology is a cascade association (Fig. 11) of:

– a two quadrants chopper (2-Q Chopper) aimed at producing a constant J current; the design of the latter is detailed in [10, 13];

– a full bridge which has been introduced in Fig. 3, and permits to inject a three level current ($-J$, 0, $+J$) into the bulb (see Fig. 12). The latter is designed according to the directions given in P. 1.2;

– a step-up high voltage transformer.

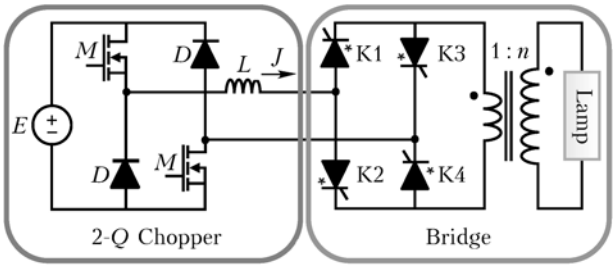

Fig. 11. Cascade topology of the square shape current generator

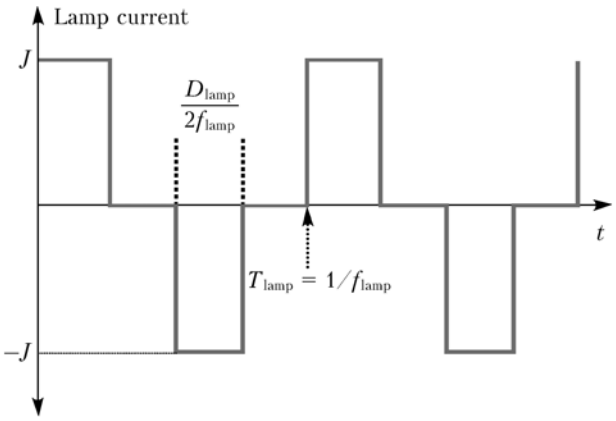

Fig. 12. Theoretical output current of the square shape generator

Accounting a 6 kV maximum voltage across the terminals of the lamp, and using 1 kV rated semiconductors (used with a 40% safety margin) for the full bridge, the step-up ratio of the transformer takes a 1 : 10 value. Its operating frequency is defined by the inverter; being dedicated to investigations and seeking the optimal conditions, a 50–200 kHz frequency range has been considered. Litz wires are used for the primary wing and mono-strand wires are used for the secondary. The gauge is selected according to the transferred power (100 W).

As developed in [14], V_{th} being the voltage across the gas when the discharge is alight, J, the magnitude of the current delivered by the current source (2-Q Chopper), and f_{lamp} and D_{lamp}, the frequency and the duty ratio of the i_{lamp} waveform controlled by the bridge, it can be established that the electrical power injected into the bulb is:

$$P_{lamp} = J D_{lamp} \frac{V_{th}}{n} - 4 f_{lamp} C_{gas} \left(\frac{V_{th}}{n} \right)^2 . \qquad (3)$$

For a given power level, any combination of these three degrees of freedom (DOF: J, f_{lamp}, and D_{lamp}) does not produce the same UV emission. Parametric investigations related to the UV emission are developed in the next section.

2.2. Using the DOF of the square shape current source to experimentally optimize the UV emission

Experimental setup

It has been observed that the UV emission level is sensitive to the operating temperature of the bulb. For this reason, considering here steady state performances, a cooling apparatus has been built, with fans organizing air circulation outside as well as through the inner pipe of the bulb. Additionally, temperature monitoring has been used and measurements of the UV emission are realized when stable temperature is observed. The UV instantaneous waveforms of this lamp (wavelength 308 nm) are captured using a THORLABS PDA-25K photo-detector, and the UV power is measured with a GIGAHERTZ-OPTIKP9710 photometer using a UV detector SN5816, configured with an integration time of 0.5 s and a dose time of 5 s, installed at 3 mm of the lamp surface.

Experimental waveforms of Fig. 13 illustrate the operation of the square shape current source generator. The primary current (i_{prim}) appears to be well controlled, as theoretically expected in Fig. 12.

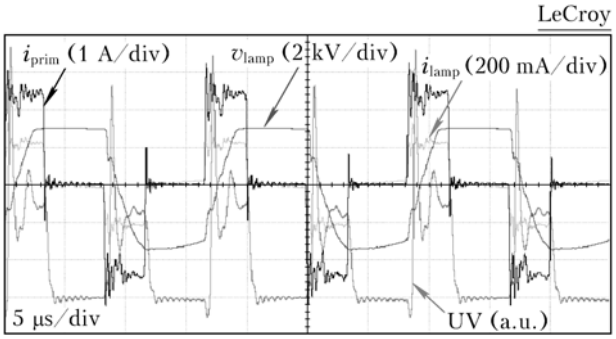

Fig. 13. Experimental performances of the square shape current source at 60 kHz: primary current i_{prim} (1 A/div), lamp current i_{lamp} (200 mA/div), and voltage V_{lamp} (2 kV/div), UV emission (a.u.); horizontal: 5 µs/div

The lamp current (i_{lamp}), although similar, suffers of relatively limited effects of the parasitic elements of the high voltage transformer. As already stated in [9], the instantaneous UV appears to be tightly correlated with the current waveform. According to equation (1), the lamp voltage (V_{lamp}) presents the expected shape.

Effect of the operating frequency

The first measurement set (Fig. 14) explores the effect of the operating frequency on the lamp efficiency: for a given current magnitude (here 100 mA), the electrical power injected into the bulb is changed, for different frequencies, using the D_{lamp} duty ratio DOF. UV power is measured at each point.

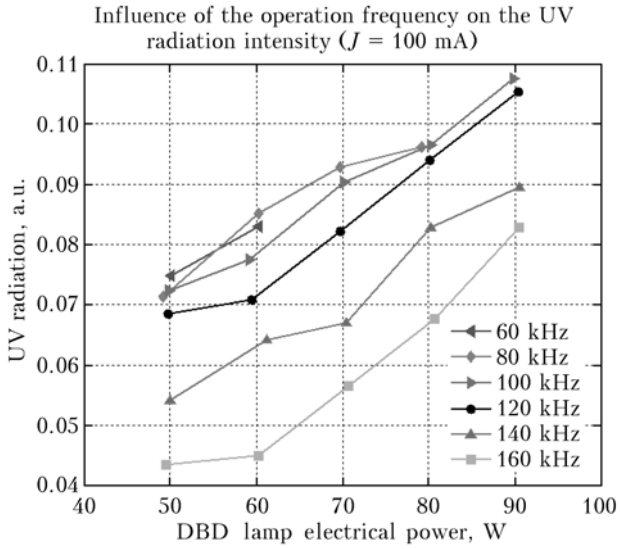

Fig. 14. XeCl lamp UV radiation power (mW/cm^2) vs. electrical power injected in the DBD. Each line corresponds to a different frequency. The power is adjusted by means of the duty ratio D_{lamp}

Curves of Fig. 14 show that the most performing conversion from electrical power to UV power is achieved in this bulb with frequencies between 60 and 80 kHz. With higher frequencies, the efficiency appears to decrease.

Effects of the current shape parameters

For a given frequency, the shape of the current injected into the lamp can be tuned by mean of two DOFs: the current magnitude J and the duty cycle, D_{lamp} (together with the operating period $1/f_{lamp}$, the latter defines the duration of the current pulses: D_{lamp}/f_{lamp}). Fig. 15 presents, for the best fitted frequency selected at the previous step (70 kHz), the UV dose obtained (over a 30 s time interval integration) with various (J, D_{lamp}) combinations.

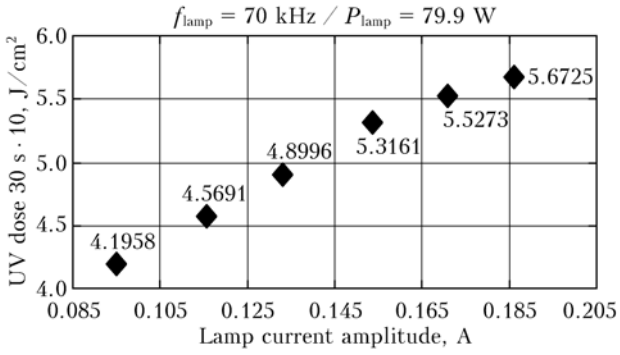

Fig. 15. UV dose at f_{lamp} = 70 kHz, P_{lamp} = 79.9 W, vs. current magnitude J (the duration of the pulses is adjusted to maintain the chosen P_{lamp} power value)

It appears from the trend shown in Fig. 15 that the highest the magnitude of the current pulses (and thus the shortest the duration of the current pulse), the most efficient will be the conversion from electrical power to UV; the difference can reach a 40% level.

Nevertheless, the actual control of these current pulses is limited by two factors. The current sizing of the semiconductor devices limits the J value. And their switching speed, as well as the leakage inductance of the transformer, which causes an overlapping phenomenon in the bridge's switching, do not allow duration shorter than a given amount (and thus limits the lowest value of the D_{lamp} parameter).

Discussion concerning the current square shape generator

From the previous parts, it clearly appears that this generator is a very flexible and valuable investigation tool, in order to determine, thanks to its three available DOFs, the most desirable supplying conditions for the DBD excilamps.

Nevertheless, its operating performances do not allow imagining using such a topology for actually supplying a DBD excilamp integrated within an industrial process. Indeed, mainly because of the switching losses in the semiconductor devices (which are operating in hard switching conditions), the global electrical efficiency of this generator hardly overcomes the 50% level; for a given operating point, the measurements and the conditions are summarized in Table 2.

Table 2

Main parameters, losses, and efficiency of the square shape current generator

Symbol	Parameter	Value
V_{in}	DC voltage level	300 V
f_{lamp}	Frequency of the current inverter	50 kHz
P_{lamp}	Lamp electrical power (measure)	56.6 W
P_{in}	Power taken from the DC source	99.6 W
η_{CVS}	Efficiency of the generator	57%
$\eta_{transfo}$	Efficiency of the sole transformer	88%

For this reason, a more performing topology is considered in the next part. The design of this new converter is especially oriented towards the optimal conditions obtained thanks to this parametric study: with the bulb used for our experimentations, we obtained finally the conditions which offer the best overall efficiency, summarized in Table 3.

Table 3

DBD lamp optimal supply conditions — values of the DOFs

Symbol	Parameter	Value
J	Lamp current magnitude	250 mA
f_{lamp}	Frequency of the lamp current	80 kHz
D_{lamp}	Duty ratio of the lamp current	25%
P_{lamp}	Lamp electrical power	70 W

3. Resonant Current source supply for DBD lamps: series inverter in discontinuous mode

3.1. Operating principle and design

According to the specifications summarized in Table 3, a series resonant inverter (SRI) operating in discontinuous mode (DCM) has been studied [5, 14, 15]. In Fig. 16, one can recognize the bridge topology, which is used to invert the lamp current. The current source associated with the latter is built by mean of a DC voltage source V_{in}, in series with a L inductor.

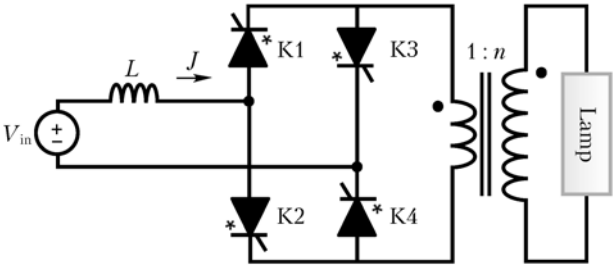

Fig. 16. Circuit of series resonant inverter in discontinuous mode

Resonant topologies have already been proposed in the literature [6, 16, 17] for lamps and DBDs control purposes. The SRI's operating principle is now analyzed; it is summarized on the waveforms of Fig. 17 and on the set of equivalent circuits presented in Fig. 18.

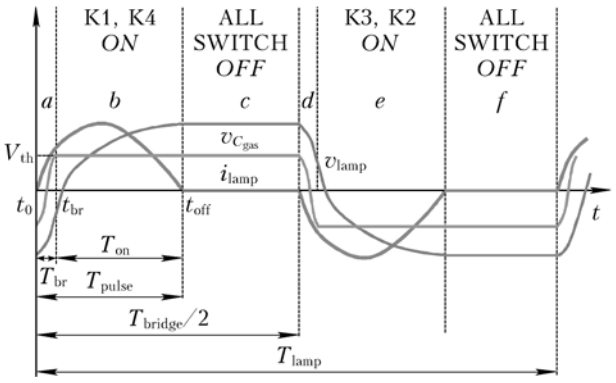

Fig. 17. Waveforms of series resonant inverter in discontinuous mode

Starting with null current in L inductor and negatively charged dielectric barriers of the bulb, switches K1 and K4 are turned *ON*.

This causes a positive half oscillating period in the resonant circuit built up with L and the capacitances of the lamp: C_{eq} (which includes the gas and the dielectric capacitance), the equivalent capacitance of the lamp when the gas is not alight (seq. *a*) or C_{gas} when the latter is *ON* (seq. *b*). This oscillation finishes when the current returns to 0 and switches K1 and K4 naturally (being unidirectional in current) turn *OFF*. The lamp voltage has been inverted during this half period.

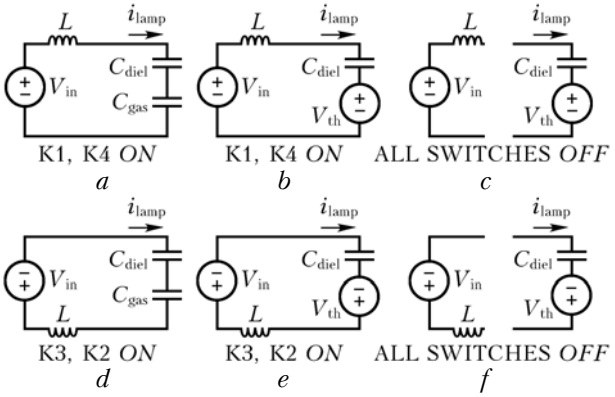

Fig. 18. Operation of series resonant inverter in discontinuous mode

All the switches remain *OFF* during a chosen time interval (seq. *c*), which depends on the value of the operating frequency; and the lamp voltage remains unchanged (positive voltage).

When switches K2 and K4 are turned *ON*, a symmetrical set of sequences (*d*, *e*, *f*) starts and produces a negative current pulse in the lamp; at the end of the latter, the lamp voltage has returned to its negative value, which is its periodic steady-state initial condition.

The characteristics of the current pulses (magnitude and duration depend on the value of the L inductor as well as on the equivalent circuit's parameters of the lamp: C_{diel}, C_{gas}, and V_{th}. Following equations (4) and (5) define the peak value of the lamp's electrical quantities; they are needed to achieve the design of the supply:

$$\hat{V}_{lamp} = V_{th} + V_{th}{}^2 C_{gas} / \left[C_{diel} (V_{th} - n V_{in}) \right]; \qquad (4)$$

$$\hat{I}_{lamp} = (\hat{V}_{lamp} \pm n V_{in}) \sqrt{C_{diel} / (n^2 L)}. \qquad (5)$$

Note: in equation (5), "–" has to be considered if the gas turns *ON* before the peak value of i_{lamp}, case *A*, right part of curves in Fig. 19, which is shown on the waveforms of Fig. 18; otherwise "+" has to be used, case *B*, left part in Fig. 19.

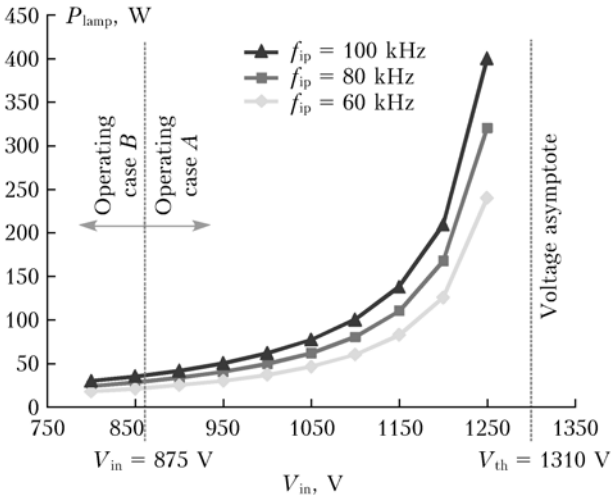

Fig. 19. Power delivered into the lamp by SRI generator: P_{lamp} vs. nV_{in} ($n = 10$) for different frequencies (60, 80, and 100 kHz)

3.2. Couplings between the supply and the DBD lamp

Analytical calculations lead to equation (6), which gives the power injected into the lamp

$$P_{\text{lamp}} = 4 f_{\text{lamp}} V_{\text{th}}^2 C_{\text{gas}} \left(\frac{V_{\text{th}}}{V_{\text{th}} - n V_{\text{in}}} - 1 \right). \qquad (6)$$

According to this equation, a stability criterion of the whole system (SRI generator + lamp) is given by relation (7):

$$n V_{\text{in}} < V_{\text{th}}. \qquad (7)$$

This condition appears in the characteristics set plotted in Fig. 19. The latter shows that, according to equation (6), two degrees of freedom, f_{lamp} and V_{in}, are available to control the power injected into the lamp.

One should also notice that formula (6) of P_{lamp} highlights the couplings of the supply and the bulb: indeed, P_{lamp} depends not only on the operating conditions defined by the inverter (f_{lamp} and V_{in}), but also on the lamp parameters (C_{gas} and V_{th}).

3.3. Experimentations and performances

An experimental setup of the SRI inverter has been designed and realized to supply the previously described Xe–Cl_2 excilamp, which parameters are given in Table 1. This power supply presents the following characteristics (Table 4).

Table 4

SRI experimental setup: main characteristics

Symbol	Parameter	Value
$\hat{I}_{\text{lamp}}$	Lamp current peak value	150 mA
f_{lamp}	Frequency of the lamp current	80 kHz
	Duration of the current pulses	μs
P_{lamp}	Lamp electrical power	75 W

As shown in Fig. 20, experimental measurements (*a*) are in very good agreement with the simulated waveforms (*b*) used for the design of the SRI inverter.

Furthermore, excellent electrical performances are achieved thanks to the proposed topology (an optimized transformer has been used for this prototype) (Table 5).

Table 5

Efficiency of SRI current generator

Symbol	Parameter	Value, %
η_{bridge}	Efficiency of H bridge + inductor	96
η_{transfo}	Efficiency of the transformer	95
η_{CVS}	Efficiency of the SRI generator	91

Additionally, very low level EMC perturbations are produced, thanks to the smooth waveforms (compared to the ones of the square shape current source).

Concerning the UV emission, the photo-detector measurements presented in Fig. 21 highlight the tight correlation between the lamp current (hence the gas conduction's current [8, 9]) and the UV emission. This property has already been shown with the square shape current source (see Fig. 13).

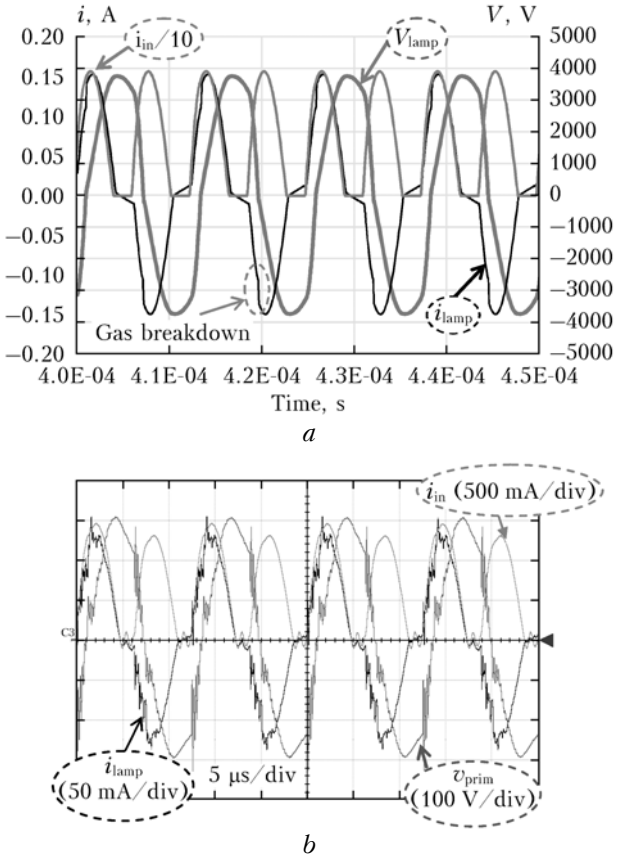

Fig. 20. Converter and DBD lamp waveforms from simulation (*a*) and from the experimental validation (*b*)

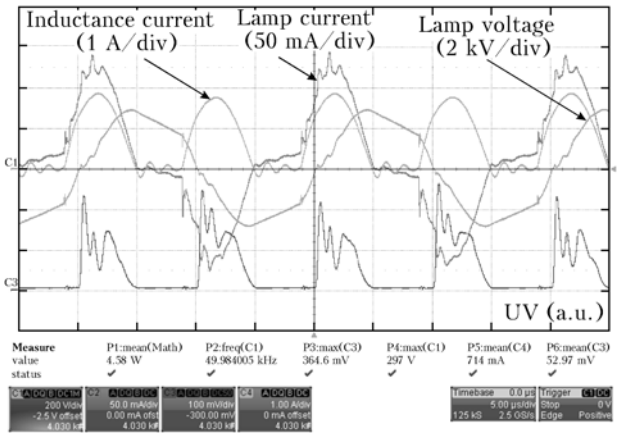

Fig. 21. Experimental measurements: electrical quantities and UV emission; horizontal: 5 μs/div

According to the experimental characteristic of Fig. 14, the adjustment of the electrical power by means of the V_{in} voltage allows to control the UV power with the best lamp efficiency (f_{lamp} being tuned to the optimal 80 kHz value).

Conclusion

For the supply of DBD UV lamps, a systemic study is carried out, in the framework of which two current controlled generators are studied and designed. The square shape one is a very valuable tool for investigating the operating conditions of the lamp. It is used to define the optimal set of parameters (current pulse magnitude and duration, frequency). But its electrical performances (efficiency, perturbations, dimensioning of the components) are rather poor. The analysis of the performances of this generator also highlights the key-role of the step up transformer in the control of the power transfers. On the basis of the parametric study, optimal supplying conditions of the selected Xe–Cl_2 excimer lamp are defined and a series resonant current inverter, operated in discontinuous mode, is studied and designed to meet these specifications with the best performances. Furthermore, it offers power adjustment capabilities, by means of two degrees of freedom (frequency and supplying voltage), which are combined with the parameters of the supplied bulb, highlighting the very tight couplings between this generator and its load.

The authors are grateful to the French-Colombian cooperation (ECOS Nord, COLCIENCIAS-ICETEX program) and to the French Midi-Pyrenees region for support.

This paper has been written on the basis of a presentation at AMPL'2013 conference (Atomic and Molecular Pulsed Lasers-2013), Tomsk, 16–20 of September.

1. *Kogelschatz U.* Dielectric-Barrier Discharges: Their History, Discharge Physics, and Industrial Applications // Plasma Chemistry and Plasma Processing. 2003. V. 23, N 1. P. 26–31.
2. *Lomaev M.I., Skakun V.S., Sosnin A., Tarasenko V.F., Shitts D.V., Erofeev M.V.* Excilamps: efficient sources of spontaneous UV and VUV radiation // Physics Uspekhi. 2003. V. 46, N 2. P. 193–209.
3. *Sosnin E.A., Oppenländer T., Tarasenko V.F.* Applications of capacitive and barrier discharge excilamps in photoscience // J. Photochemistry and Photobiology C: Photochemistry Reviews. 2006. V. 7, N 4. P. 145–163.
4. *Diez R., Salanne J.-P., Piquet H., Bhosle S., Zissis G.* Predictive model of a DBD lamp for power supply design and method for the automatic identification of its parameters // The European Physical J. Phys. D: Appl. Phys. 2007. V. 37, N 3. P. 307–313.
5. *Lopez A.M., Piquet H., Patino D., Diez R., Bonnin X.* Parameters Identification and Gas Behavior Characterization of DBD Systems // IEEE Trans. on Plasma Science. 2013. V. 41, N 8. P. 2335–2342. DOI: 10.1109/TPS.2013.2273462.
6. *Mildren R., Carman R., Falconer I.* Visible and VUV emission from a xenon dielectric barrier discharge using pulsed and sinusoidal voltage excitation waveforms // IEEE Trans. on Plasma Science. 2002. V. 30. P. 192–193.
7. *Williamson J.M., Trump D.D., Bletzinger P., Ganguly B.N.* Comparison of high-voltage ac and pulsed operation of a surface dielectric barrier discharge // J. Phys. D: Appl. Phys. 2006. V. 39. P. 4400–4406.
8. *Diez R., Piquet H., Cousineau M., Bhosle S.* Current-Mode Power Converter for Radiation Control in DBD Excimer Lamps // IEEE Trans. on Industrial Electronics. 2012. V. 59, N 4. P. 1912–1919.
9. *Piquet H., Bhosle S., Diez R., Erofeev M.* Pulsed Current-Mode Supply of Dielectric Barrier Discharge Excilamps for the Control of the Radiated Ultraviolet Power // IEEE Trans. on Plasma Science. 2010. V. 38, N 10. P. 2531–2538.
10. *Bonnin X., Piquet H., Naudé N., Bouzidi M.C., Gherardi N., Blaquière J.-M.* Design of a current converter to maximize the power into homogeneous dielectric barrier discharge (DBD) devices // The European Physical J. Appl. Phys. 2013. V. 64. P. 10901. DOI: 10.1051/epjap/2013130080.
11. *Cousineau M., Diez R., Piquet H., Durrieu O.* Synthesized High-Frequency Thyristor for Dielectric Barrier Discharge Excimer Lamps // IEEE Trans. on Industrial Electronics. 2012. V. 59, N 4. P. 1920–1928.
12. *Bonnin X., Piquet H., Diez R., Florez D.* Designing the high voltage transformer of power supplies for DBD: Windings arrangement to reduce the parasitic capacitive effects // 15th European Conference on Power Electronics and Applications (EPE). 2013. P. 1–9. DOI: 10.1109/EPE.2013.6631928
13. *Flórez D., Diez R., Hay K., Piquet H.* DBD Excimer Lamp Power Supply with Fully Controlled Operating Conditions // OPTIM Conf., IEEE. 2012.
14. *Flórez D.* Power supplies for the study and efficient use of DBD excimer lamps // PHD thesis from University of Toulouse (France). January, 2014.
15. *Chéron Y.* Soft Commutation. London: Chapman & Hall, 1992.
16. *Kalisiak S., Holub M., Jakubowski T.* Resonant inverter with output voltage pulse-phase-shift control for DBD plasma reactor supply // 13th European Conf. on Power Electronics and Applications, EPE'09. 2009.
17. *Alonso J., Garcia J., Calleja A., Ribas J., Cardesin J.* Analysis, design, and experimentation of a high-voltage power supply for ozone generation based on current-fed parallel-resonant push-pull inverter // IEEE Trans. on Industry Applications. 2005. V. 41, N 5. P. 1364–1372.
18. *Meisser M., Kling R., Heering W.* Universal Resonant Topology for High Frequency Pulsed Operation of Dielectric Barrier Discharge Light Sources // Applied Power Electronics Conf. and Exposition (APEC). Twenty-Sixth Annual IEEE, 2011.
19. *Flórez D., Diez R., Piquet H.* Series-resonant inverter in DCM mode for the supply of a DBD excimer UV lamp // Industry Applications Society Annual Meeting (IAS). IEEE. 2012. P. 1–8.